⊙ 研究論文

Two-Parameter Characterization for the Resistance Curves of Ductile Crack Growth

S. K. Jang* · X. K. Zhu**

연성균열성장 저항곡선에 대한 2매개변수의 특성

장 석 기* · X. K. Zhu**

Key words : Ductile Crack Growth, Initiation Toughness, J-R Curve, J-A_2 Solution, Constraint Effect

Abstract

The present paper considers the constraint effect on J-R curves under the two-parameter J-A_2 controlled crack growth within a certain amount of crack extension. Since the parameter A_2 in J-A_2 three-term solution is independent of applied loading under fully plasticity or large-scale deformation, A_2 is a proper constraint parameter uring crack extension. Both J and A_2 are used to characterize the resistance curves of ductile crack growth using J as the loading level and A_2 as a constraint parameter. Approach of the constraint-corrected J-R curve is proposed, and a procedure of transferring the J-R curves determined from standard ASTM procedure to non-standard specimens or real cracked structures is outlined.

The test data (e.g. initiation toughness J_{IC} and tearing modulus T_R) of Joyce and Link(Engineering Fracture Mechanics, 1997, 57(4) : 431-446) for single-edge notched bend [SENB] specimen with from shallow to deep cracks is employed to demonstrate the efficiency of the present approach. The variation of J_{IC} and T_R with the constraint parameter A_2 is obtained and a constraint-corrected J-R curve is constructed for the test material of HY80 steel. Comparisons show that the predicted J-R curves can very well match with the experimental data for both deep and shallow cracked specimens over a reasonably large amount of crack extension.

Finally, the present constraint-corrected J-R curve is used to predict the crack growth resistance curves for different fracture specimens. The constraint effects of specimen types and specimen sizes on the J-R curves can be easily obtained from the constrain-corrected J-R curves.

* Department of Marine Engineering Mokpo National Maritime University(receipt : '99. 3.)
** Department of Mechanical Enginneering University of South Carolina

1. Introduction

The fracture toughness J_{IC} and J-integral resistance curves (J-R curves) have been widely used in the integrity assessment of engineering structures in the presence of crack ductile tearing. The J-integral values are also used as indexes of material toughness for alloy design, materials processing, materials selection and specification and quality assurance. Thus, the initiation toughness J_{IC} and J-R curves obtained from laboratory must be accurate and applicable into real cracked structures. The strict size requirements are specified in fracture test standards, such as ASTM fracture test standards E1737-96 (1996)[2], restrict current fracture design and inspection methods to the application of geometry-independent data. The measurement of the fracture toughness J_{IC} and J-R curves usually used standard specimen geometry with high crack-tip constraint, such as the deeply cracked three-point bend [3PB] specimens and compact tension [CT] specimens. However, most of real cracked structures belong to the group of low constraint crack geometry. Therefore, the constraint effects of specimen geometry and loading configuration on the J-R curves must be considered so as to transfer the J-R curves determined in laboratory to application for real cracked structures.

The standard J-R curve consists of a plot of J-integral versus crack extension in the region of J-controlled growth and is size-independent, as specified in ASTM fracture test standards E1737-96 (1996). But for non-standard or low constraint specimens, J-R curves could be size - dependent due to the loss of J-control. Generally, fracture properties, such as fracture toughness J_{IC} and the J-R curve, could be functions of test specimen geometry, size, thickness and loading configurations. In the passed years, a large number of nonstandard fracture specimens were measured to investigate the effect of crack-tip constraints on these fracture properties of ductile growing cracks. For the ASTM 710 Grade A steel, Hancock *et al.* (1993)[11] measured the fracture toughness J_{IC} and J-R curves for the specimens of 3PB, CT, center cracked panel [CCP] in tension and surface cracked panel [SCP] in tension with different crack depths. For A533B, HY-100 and HY-80 structure steels, Joyce and Link (1995, 1997)[14,15] presented the experiment data of ductile crack extension for the specimens of 3PB, CT, single edge-notched bend [SENB] specimen, single edge-notched tensile [SENT] specimen, double edge-cracked plate [DECP] in tension with shallow to deep cracks. Both groups used several types of specimens in order to achieve different crack tip constraint conditions. These investigators could not find any significant constraint effect on growth initiation, but they observed a larger constraint effect on the slop of J-R curve after some relatively large amount of growth. The same results are observed from ductile crack extension experiments by Marschall *et al.* (1989)[20], Eisele *et al.* (1992)[8] and Roos *et al.* (1993)[23] for large-sized fracture specimens, and by Elliot *et al.*, 1991[9] ; Alexander, 1993[1], Yoon *et al.*, 1995[31] for very small or sub-sized fracture specimens. Other similar experimental results are also reported by Kordisch *et al.* (1989)[18], Kelmm *et al.* (1991)[17], Roos *et al.* (1991)[24], Henry *et al.* (1996)[13], Haynes and Gangloff (1997)[12] and so on.

All experimental data has suggested that the J-R curves vary with the level of constraints. As shown in Fig. 1, the J-R curves for high constraint specimen geometry is lower than those for low constraint specimen geometry. In other words, the slope of J-R curves after crack initiation decreases with increasing local constraint

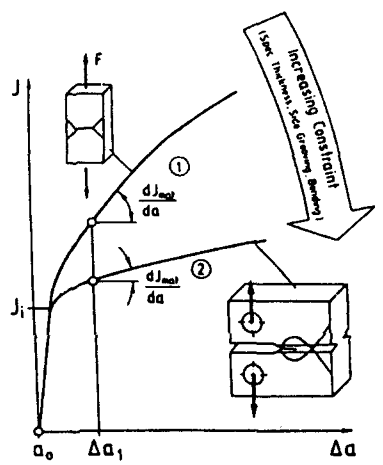

Fig. 1 Variation of *J-R* curves with the level of crack-tip constraints

ahead of the crack tip. To simulate the experimental results of ductile crack growth, two and three dimensional finite element analyses [FEA] were carried out (cf. Yuan and Brocks, 1989 ; Brocks *et al.*, 1994[4] ; Xia *et al.*, 1995[27] ; Faleskog, 1995[10] ; Henry *et al.*, 1996[13] ; Shan *et al.*, 1996[25] ; Kikuchi, 1997[16] ; Yan and Mai, 1997[28]). FEA simulations for different fracture specimens, such as CT, 3PB, SENB, SENT and CCP, show that ductile crack growth is sensitive to the crack-tip constraints, the mount of J-controlled crack growth is different for different specimens. At the stage of initiation, the fracture toughness J_{IC} increases somewhat with the decreasing crack lengths or crack-tip constraints, and weakly linearly related to constraint level.

During crack growth, the tearing resistance of J-R curve increases with decreasing constraint level, and has a linear relation with the constraint or triaxiality. Nevertheless, these FEA simulations depend on the test data and crack growth criterion during the entire crack growth, and used different constraint parameters. A simple approach to reproduce J-R curves and an appropriate parameter to quantify the magnitude of constraints need to develop further.

The effect of constraints on crack-tip fields is quite extensively studied and reported for a stationary elastic-plastic crack with different geometry and loading configurations. Most recently, Chao and Zhu (1998)[7] reviewed the research advances in more details. The three main methods to quantify crack-tip constraints are J-T approach proposed by Betegon and Hancock (1991)[3], J-Q approach proposed by O' Dowd and Shih (1991, 1992)[21,22], J-A_2 approach proposed by Yang *et al.* (1993)[29] and Chao *et al.* (1994)[5]. The J-T approach has only limited use in elastic-plastic fracture analysis because it is based on the elasticity theory. The J-Q approach is only good for small applied loads because the parameter Q is distance-dependent under large applied loads (Sharma *et al.*, 1995[26]). However, J-A_2 approach is a rigorous three-term asymptotic solution. A_2 is nearly independent of its position near the crack tip (Nikishkov *et al.*, 1995[19]) and is successfully used to quantify the constraints of crack-tip fields for different geometry and loading configurations (Chao *et al.*, 1994[5] ; Chao and Zhu, 1998[7] ; Zhu and Chao, 1999[33]). Accordingly, the J-A_2 approach is a preferable methodology and A_2 is a proper constraint parameter. For a ductile growing crack, similar to the concept of J-controlled crack growth, one can envision that under certain amount of crack extension the J-A_2 description can approximately characterize the effect of crack-tip constraints on ductile crack growth with J being the driving force and A_2 a constraint parameter. The amount of J-A_2 controlled crack growth is much larger than that of the J-controlled crack growth since the zone dominated by J-A_2 at the crack tip is much larger than that controlled by J alone (Chao and Zhu, 1998[7]).

The purpose of this work is to extend the J-A_2 characterization of crack-tip fields to the stable crack growth region using J as the loading level and A_2 as a constraint parameter. A procedure of transferring the J-R curves determined from standard ASTM procedure to non-standard specimen or flawed structures is outlined. Approach of a constraint-corrected J-R curve is presented and a set of test data by Joyce and Link (1997)[15] is employed to demonstrate the present approach. Comparisons between predicted and experimental J-R curves, and applications of the constraint-corrected J-R curves are given in this work.

2. Constraint correction of crack-tip fields

Our attention is focused on mode-I cracks in elastic-plastic materials under the plane strain conditions. The material behavior is described by Ramberg-Osgood power-law strain hardening curve where the uniaxial strain, ε is related to the uniaxial stress, σ in simple tension by

$$\frac{\varepsilon}{\varepsilon_0}=\frac{\sigma}{\sigma_0}+\alpha\left[\frac{\sigma}{\sigma_0}\right]^n \tag{1}$$

where σ_0 is a yield stress, $\varepsilon_0=\sigma_0/E$ is a yield strain with E as Young' s modulus, α is a material hardening constant and n is a strain hardening exponent. By use of J_2 deformation theory of plasticity, the uniaxial stress-strain relation (1) can be generalized to multi-axial states as follows

$$\frac{\varepsilon_{ij}}{\varepsilon_0}=(1+\nu)\frac{\sigma_{ij}}{\sigma_0}-\frac{\sigma_{kk}}{\sigma_0}\delta_{ij}+\frac{3}{2}\alpha\left(\frac{\sigma_e}{\sigma_0}\right)^{n-1}\frac{S_{ij}}{\sigma_0} \tag{2}$$

where ν is the Poisson' s ratio, δ_{ij} is the Kronecker delta, S_{ij} is the deviatoric stress and σ_e is the von Mises effective stress defined as $\sigma=\sqrt{3S_{ij}S_{ij}/2}$

2.1 J-A_2 three-term asymptotic solution

Using the deformation plasticity theory (2) and referring to the polar coordinates r and θ centered at the crack tip with θ=0 corresponding the uncracked ligament, Yang *et al.* (1993)[30] and Chao *et al.* (1994)[5] developed a three-term asymptotic crack-tip field with only two parameters J and A_2. In which J-integral quantifies the magnitude of applied loading and A_2 describes crack-tip constraints. The asymptotic stress, strain and displacement fields can be written as follows

$$\frac{\sigma_{ij}}{\sigma_0}=A_1\Big[\left(\frac{r}{L}\right)^{s_1}\tilde{\sigma}_{ij}^{(1)}(\theta,n)+A_2\left(\frac{r}{L}\right)^{s_2}\tilde{\sigma}_{ij}^{(2)}(\theta,n)+A_2^2\left(\frac{r}{L}\right)^{s_3}\tilde{\sigma}_{ij}^{(3)}(\theta,n)\Big] \tag{3}$$

$$\frac{\varepsilon_{ij}}{\alpha\varepsilon_0}=A_1^n\Big[\left(\frac{r}{L}\right)^{ns_1}\tilde{\varepsilon}_{ij}^{(1)}(\theta,n)+A_2\left(\frac{r}{L}\right)^{(n-1)s_1+s_2}\tilde{\varepsilon}_{ij}^{(2)}(\theta,n)+A_2^2\left(\frac{r}{L}\right)^{(n-1)s_1+s_3}\tilde{\varepsilon}_{ij}^{(3)}(\theta,n)\Big] \tag{4}$$

$$\frac{u_i}{\alpha\varepsilon_0 L}=A_1^n\Big[\left(\frac{r}{L}\right)^{ns_1+1}\tilde{u}_i^{(1)}(\theta,n)+A_2\left(\frac{r}{L}\right)^{(n-1)s_1+s_2+1}\tilde{u}_i^{(2)}(\theta,n)+A_2^2\left(\frac{r}{L}\right)^{(n-1)s_1+s_3+1}\tilde{u}_i^{(3)}(\theta,n)\Big] \tag{5}$$

where the parameters A_1 and s_1 from the HRR fields are given by

$$A_1=\left(\frac{J}{\alpha\varepsilon_0\sigma_0 I_n L}\right)^{-s_1},\ s_1=\frac{-1}{n+1} \tag{6}$$

and $s_3=2s_2-s_1$ for $n\geq 3$. The angular functions $\tilde{\sigma}_{ij}^{(k)}$, $\tilde{\varepsilon}_{ij}^{(k)}$ and $\tilde{u}_i^{(k)}$, the stress power exponents s_k and the dimensionless integration constant I_n are only dependent of the hardening exponent n and independent of the other material constants (i.e. α, ε_0, σ_0) and applied loads.

For the plane strain mode-I cracks, the dimensionless functions $\tilde{\sigma}_{ij}^{(k)}$, $\tilde{\varepsilon}_{ij}^{(k)}$, $\tilde{u}_i^{(k)}$, s_k, and I_n have been calculated and tabulated by Chao and Zhang (1997)[6]. L is a characteristic length parameter which can be chosen as the crack length a, the specimen width W, the thickness B or unit 1 cm. A_2 is an undetermined parameter and may be related to the loading and geometry of specimen. When $A_2=0$, the three-term asymptotic solutions (3)−(5) reduce to the leading-term HRR field. In other words, the first-order field of the three-term asymptotic solution is the HRR singularity field.

Yang *et al.* (1993)[30] showed that for moderate to low hardening materials, i.e. $n \geq 3$, the above three-term asymptotic solutions are the fully plastic or pure power-law solutions. Comparing with finite element results, Chao *et al.* (1994)[5], Chao and Zhu (1998)[7] as well as Zhu and Chao (1999)[33] indicated that the three-term solution can be used to characterize the stress and deformation in a crack tip region well beyond $r/(J/\sigma_0)=5$. Furthermore the J-A_2 three-term solution is universally valid in both small scale yielding and large scale yielding, low constraint and high constraint crack geometry, and low and high strain hardening materials.

As pointed by Yang (1993)[29] and Chao *et al.* (1994)[5], *the constraint parameter A_2 in the three-term solutions* (3)−(5) *is a distance -independent constant within* $1<r(J/\sigma_0)<5$ *and independent of applied J under fully plastic deformation.* Mathematically speaking, A2 only is the function of strain hardening exponent n and geometry dimension (a, W, a/W), namely

$$A_2 \mid_{\text{fully plastic}} = f(n, geometry) \tag{7}$$

Using finite element analysis, these authors obtained the values of constraint parameter A_2 corresponding to different levels of applied J. The values of A_2 become a constant as the applied load increases beyond about 1.2 limit load for all specimens with different hardening exponents. At the load level, J_C, corresponding to crack initiation, it was showed that the values of A_2 at are close to those under fully plastic conditions. For a crack specimen under large-scale yielding or near fully plastic deformation, the value of A_2 determined at $J=J_C$ can remain constant for other applied loads $J \geq J_C$. Therefore, it is specially appropriated to use A_2 as a constraint parameter during J-A_2 controlling crack growth.

2.2 Determination of the constraint parameter A_2

The constraint parameter A_2 depends on cracked specimen geometry, strain hardening exponent and loading type for an arbitrary crack problem. A_2 is a free constant in asymptotic analysis and can be determined by far-field solutions. Yang *et al.* (1993)[30] and Chao *et al.* (1994)[5] determined A_2 using a point matching technique, i.e. the stress value from finite element analysis at a point (r, θ) is set equal to the three term analytical solution (3) to yield the A_2 value. Specially, these authors used σ_{rr} and $\sigma_{\theta\theta}$ at $r=2(J/\sigma_0)$, $\theta=0°$ or 45° to determine A_2. Chao and Zhu (1998)[7] also used this approach to determine A_2 but r is chosen from J/σ_0 to $5(J/\sigma_0)$ such as :

$$A_1\Big[\Big(\frac{r}{L}\Big)^{s_1}\tilde{\sigma}_{\theta\theta}^{(1)}(\theta,n) + A_2\Big(\frac{r}{L}\Big)^{s_2}\tilde{\sigma}_{\theta\theta}^{(2)}(\theta,n) + A_2^2\Big(\frac{r}{L}\Big)^{s_3}\tilde{\sigma}_{\theta\theta}^{(3)}(\theta,n)\Big] - \frac{\sigma_{\theta\theta}^{FEA}}{\sigma_0} = 0 \tag{8}$$

or equivalently

$$aA_2^2 + bA_2 + c = 0 \tag{9}$$

where

$$a=\left(\frac{r}{L}\right)^{s_3}\tilde{\sigma}_{\theta\theta}^{(3)}(\theta) \tag{10a}$$

$$b=\left(\frac{r}{L}\right)^{s_2}\tilde{\sigma}_{\theta\theta}^{(2)}(\theta) \tag{10b}$$

$$c=\left(\frac{r}{L}\right)^{s_1}\tilde{\sigma}_{\theta\theta}^{(1)}(\theta)-\left(\frac{J}{\alpha\varepsilon_0\sigma_0 I_n L}\right)^{s_1}\frac{\sigma_{\theta\theta}^{FEA}(r,\theta)}{\sigma_0} \tag{10c}$$

in (8)–(10), $J/\sigma_0 \leq r \leq 5(J/\sigma_0)$ and $\theta=0^\circ$ or 45°, $\sigma_{\theta\theta}^{FEA}$ is the hoop stress from FEA calculations. A_2 can be simply determined by solving the above two-order equation (8) or (9). Yang *et al.* (1993)[30], Chao and Zhu (1998)[7] have demonstrated that the A_2 values determined from these different positions are only somewhat different. More accurate method to determine the distance-independent A_2, one can use the least square procedure, i.e. fitting the finite element data with the analytical solutions, developed by Nikishkov *et al.* (1995)[16]. This technique showed that A2 is almost independent of its location in the interested region of $1 < r/(J/\sigma_0) < 5$.

3. Constraint correction of resistance curves of ductile crack growth

The three-term asymptotic solution (3)–(6) with two-parameter J and A_2 has been successfully used to quantify the effects of constraint on the stationary crack-tip fields for different geometry and loading configurations (Yang *et al.*, 1993[30]; Chao, *et al.*, 19945); Zhu and Chao, 1999[33]). For growing cracks, similar to the concept of J-controlled crack growth, one can envision that under certain amount of crack extension the J-A_2 description can approximately characterize the effects of geometry constraint on ductile crack growth with J being the driving force and A_2 the constraint parameter. The amount of J-A_2 controlled crack growth is much larger than that of the J-controlled crack growth since the zone dominated by J-A_2 at the crack tip is much larger than that controlled by J alone (Chao and Zhu, 1998[7]).

In this section we first present a general procedure of transferring the J-R curves determined from standard ASTM procedure to non-standard specimen or flawed structures by J-A_2 description. Then based on the test data (e.g. initiation toughness JIC and tearing modulus T_R) of Joyce and Link (1997)[15] for single-edge notched bending [SENB] specimen with from shallow cracks to deep cracks, a prediction of J-R curve containing the constraint parameter A_2 is presented.

3.1 Approach of constraint-corrected *J-R* curves

Under conditions of crack-tip plane strain, the fracture toughness is characterized by the J-Integral as defined by the test standard in ASTM E 1737-96. Based on the amount of crack extension, three toughness properties are identified as : (a) instability without significant prior crack extension (J_C) ; (b) onset of stable crack extension (J_{IC}) ; (c) stable crack growth resistance curve (J-R) in the region of J-controlled growth. The interest of this work is focused on stable crack growth.

Since J_{IC} is corresponding to the crack initiation, the constraint parameter A_2 can be solved by equation (8) using the three-term solution (3) to match with finite element results at this load level. For different constraint specimens (ASTM standard or non-standard specimens, such as CT, SENB, SENT, DECT, CCP) with same material properties, once J_{IC} is measured, the corresponding A_2 can be obtained by equation (8) and FEA results at the initiation load. ASTM standard E 1737-962) specifies that the initiation toughness J_{IC} is the J-integral $\Delta a_Q=\frac{J_{IC}}{2\sigma_F}+0.2$

(mm). As such, one can fit a curve between the initiation toughness J_{IC} and the constraint parameter A_2 of various specimens as follows

$$J_{IC}(A_2)=J(\Delta a_Q, A_2)\ \Big|_{\Delta a_Q=\frac{J_{IC}}{2\sigma_F}+0.2(mm)} \tag{11}$$

where Δ_{aQ} is the crack extension at J_{IC}, σ_F is the flow stress or effective yield stress.

As described in previous section, under large-scale yielding or near fully plastic deformation the constraint parameter A_2 determined at $J=J_{IC}$ remain constant for $J\geq J_{IC}$. If the crack extension occurs within the range of the J-A_2 controlled growth, the value of A_2 is approximately invariable for a specific specimen. Based on the standard procedure of ASTM E 1737-96, the J versus crack growth behavior is approximated by a best-fit power-law relationship. After considering constraint effects on a growing crack tip, a curve of J versus crack extension Δa under J-A_2 controlled growth is assumed in this paper as

$$J(\Delta a, A_2)=C_0(A_2)+C_1(A_2)\left(\frac{\Delta a}{k}\right)^{C2(A2)} \tag{12}$$

where k=1mm or 1 in. which depends on the unit of Δa. The coefficients $C_0(A_2)$, $C_1(A_2)$, $C_2(A_2)$ are unknown constants and dependent of the constraint at crack tip for a specific material and specimen. It should be noted that Equation (12) considers the non-zero crack extension resistance at the beginning of $\Delta a=0$. If one knows the initial crack growing condition, e.g. $J(\Delta a, A_2)=J_0(A_2)$ as $\Delta a=0$, from the test data, then from (12) one has

$$C_0(A_2)=J_0(A_2) \tag{13}$$

Generally speaking, if three test points (J_i, Δa_i) ($i=1-3$) on each experimental J-R curve are given, the three coefficients in (12) can be determined by

$$J_i(\Delta a_i, A_2)=C_0(A_2)+C_1(A_2)\left(\frac{\Delta a_i}{k}\right)^{C2(A2)},\ (i=1-3) \tag{14}$$

ASTM standard E 1737-96 specifies that $J(\Delta a=0)$ as $\Delta a=0$, i.e. $J_0(A_2)=0$, and the tearing resistance, $T_R=\frac{E}{\sigma_0^2}\frac{dJ}{da}$ or the slop dJ/da of the J-R curve need to be given at $\Delta a=1mm$. Accordingly, from (13), $C_0=0$. From (11) and (12), one obtains the governing equation to determine the unknown constants C_1 and C_2 as follows

$$C_1(A_2)\left(\frac{J_{IC}}{2k\sigma_F}+0.2\right)^{C2(A2)}=J_{IC}(A_2)-J_0(A_2)$$
$$C_1(A_2)C_2(A_2)\left(\frac{\Delta a_i}{k}\right)^{C_2(A_2)-1}=\frac{\partial J(\Delta a, A_2)}{\partial a}\Big|_{\Delta a=\Delta a_i} \tag{15}$$

For a specific A_2 value, e.g. A_2 from 0 to -1.0, to solve equations (14) or (15) gives the solutions to constants C_1 and C_2, then we can fit the correlated curves of C_1-A_2 and C_2-A_2. Up to now, the J-R curve (12) with the parameter A_2 is constructed or determined completely. For convenience, Equation (12) is referred to as constraint-corrected J-R curves thereafter. For non-standard specimens or real structures, once the constraint parameter A_2 is determined, the J-R curves of these geometries can then be obtained from Equation (12).

As a summary, Figure 2 illustrates the procedure to construct constraint-corrected J-R curves based on ASTM fracture test standards : J-R curves are determined experimentally based on ASTM standard for different crack sizes or specimen types, as shown in Fig. 2(a). The test results can be typically chosen from several low constraint to high constraint specimens (three sets of data at least). Then at the initiation load of J_{IC}, FEA is performed to determine the constraint parameter A_2 at the crack tip using

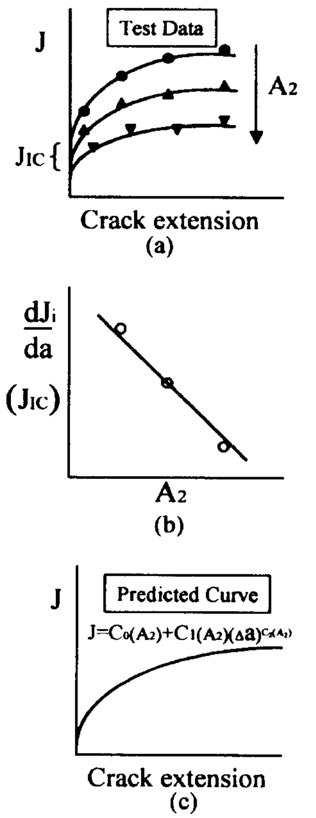

Fig. 2 Analysis procedure of constraint-corrected *J-R* curves
(a) Experimental *J-R* curves
(b) Correlation between the slope of *J-R* curves or J_{IC} and A_2
(c) Predicted *J-R* curves with the parameter A_2

equation (8).

Through curve fitting, could be linearly, one can determine the correlation between the constraint parameter A_2 and the initiation toughness J_{IC}, or the slope of *J-R* curves dJi /da for a specific crack extension Δa, as shown in Fig. 3(b).

Using the fitting curves : J_{IC}-A_2, dJ$_i$/da-A_2, one can obtain a power-law curve of crack growth resistance J versus crack extension Δa, as shown in Fig. 3(c) and equation (12). This constraint-corrected *J-R* curve can predict *J-R*

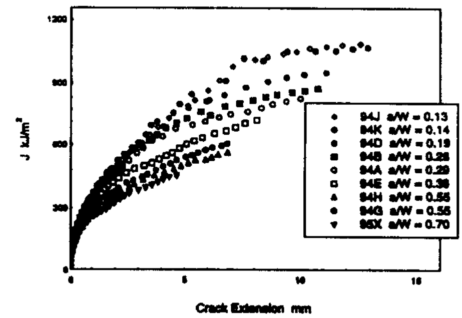

Fig. 3 Experimental *J-R* curves for standard and shallow crack SENB specimens (Joyce and Link, 1997)

curves quantified the crack-tip constraint by the parameter A_2.

3.2 Experimental results of SENB specimens

The shallow cracked SENB specimen can exhibit as low a constraint condition as any found in structure applications and can be tested much easier than the other low constraint specimens such as SENT, DECP, CCP. Therefore, the toughness test of SENB from shallow to deep cracks can give a wide of constraint levels for the tested material from low to high constraints. This section introduces several sets of test data about SENB specimens.

Joyce and Link (1997)[15] tested a series of SENB specimens with a/W ratios varying from o.13 to 0.83 for an HY80 steel. These specimens were all 1T SENB with 20% side grooves as recommended by ASTM E 1737-96. The material properties are the 0.2% yield strength σ_0=610MPa, the ultimate strength σ_{us}=726MPa, the Young' s modulus E=199 GPa, the Poisson ratio ν=0.29 and the strain hardening exponent n=10.

The experimental *J-R* curves for the HY80 steel specimens tested by Joyce and Link (1997)[15] are shown in Fig. 3 and Fig. 4. Figure 3 shows specimens with $a/W \leq 0.7$, i.e. the specimens which satisfy the initial crack length

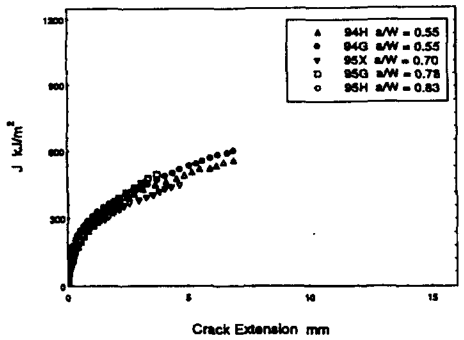

Fig. 4 Experimental *J-R* curves for standard and deep crack SENB specimens (Joyce and Link, 1997)

requirements in ASTM E 1737-96 and those with shorter cracks. While Fig. 4 shows specimens with $a/W \geq 0.5$, i.e. the specimens which satisfy the initial crack length requirements in ASTM E 1737-96 and those with longer cracks. In both cases the non-standard crack length geometries give higher *J-R* curves than the standard geometires. The *J-R* curves of the standard specimens with $0.55 \leq a/W \leq 0.70$ form a tight band of data with little dependence on a/W. The dependence of crack length on the *J-R* curves is attributed here to be due to the difference in crack-tip constant.

The initiation toughness J_{IC} and the material tearing resistance $T_R = \frac{E}{\sigma_0^2}\frac{dJ}{da}$ at $\Delta a = 1mm$ are presented by Joyce and Link (1997)[15] for all specimens and listed in Table 1. Based on *J-Q* approach (O' Dowd and Shih, 1991)[21], they estimated the *Q*-constraint parameter for all specimens with the *J*-integral at the J_{IC} level and listed the values of *Q*-parameter in Table 1. As mentioned earlier, the parameter *Q* depends on the load level and the distance ahead of the crack tip (Sharma *et al.*, 1995[26] ; Faleskog, 1995[10]), and so *Q* is a "rough" constraint parameter. The more proper constraint parameter A_2, used in this work, is almost independent of the distance ahead of the crack tip in the interested region of $1 < r/(J/\sigma_0) < 5$ and independent of loading under the large scale deformation. From the definition of Q, i.e. $Q\sigma_0 = \sigma_{\theta\theta} - \sigma_{\theta\theta}^{HRR}$ at $\theta = 0$ and $r = 2J/\sigma_0$, and comparing to (3), we can obtain the transformation relationship of Q and A_2

$$A_2\left(\frac{2J}{\sigma_0 L}\right)^{s_2} \tilde{\sigma}_{\theta\theta}^{(2)}(0) + A_2^2\left(\frac{2J}{\sigma_0 L}\right)^{s_3} \tilde{\sigma}_{\theta\theta}^{(3)}(0)$$

$$= Q\left(\frac{J}{\alpha\varepsilon_0\sigma_0 I_n L}\right)^{s_1} \qquad (16a)$$

For n=10, the constants $s_1 = -0.06977$, $s_2 = 0.06977$, $s_3 = 0.23044$, $I_n = 4.53985$, $\tilde{\sigma}_{\theta\theta}^{(2)} = 0.3130$, $\sigma_{\theta\theta}^{(3)}(0) = -6.4127$. For the HY80 steel, the yield stress $\sigma_0 = 610MPa$, the yield strain $\varepsilon_0 = \sigma_0/E = 0.003065$. Letting $\alpha = 1$ and $L = 10mm$, (16a) becomes

$$0.313\left(\frac{J}{3050}\right)^{0.06977}$$

$$A_2 - 6.4127\left(\frac{J}{3050}\right)^{0.23044}$$

$$A_2^2 = \left(\frac{84.882}{J}\right)^{0.09091} Q \qquad (16b)$$

Using (16b), we can convert the values of Q to the values of A_2. The evaluated results of A_2 for all specimens are also listed in Table 1.

3.3 Constraint-corrected *J-R* curves for HY80 steel

Using the test data in Table 1 and following the procedures described in Section 3.1, we can predict a constraint-corrected *J-R* curve using the parameter A_2. Figures 5(a) and 5(b) show plots of J_{IC} and T_R versus constraint level as quantified by A_2. Figure 5(a) shows that the initial toughness J_{IC} can be approximately considered as a constraint-independent constant. This corroborates the experimental observations of Hancock *et al.* (1993)[11], Joyce and Link (1995, 1997)[14, 15]. Thus the relationship of J_{IC} versus A_2 can be approximated by an average constant

Table 1. Fracture toughness and constraint quantities for all SENB specimens

Specimen I.D.	a/W	a/b (mm)	J_{IC} (KJ/m²)	T_R ($\Delta a=1mm$)	Q	A_2
94A	0.29	14.5/35.5	211.8	95.8	−0.36	−0.274
94B	0.26	13.0/37.0	225.6	99.1	−0.43	−0.299
94D	0.19	9.5/40.5	217.2	104.0	−0.60	−0.362
94E	0.39	19.5/30.5	216.0	77.9	−0.24	−0.217
94G	0.55	27.5/22.5	195.2	72.1	−0.15	−0.168
94H	0.55	27.5/22.5	169.2	71.1	−0.10	−0.134
94J	0.13	6.5/43.5	219.3	109.4	−0.70	−0.393
94K	0.14	7.0/43.0	215.1	117.4	−0.70	−0.394
94K	0.14	7.0/43.0	183.0	100.0	−0.67	−0.395
94J	0.13	6.5/43.5	196.5	108.7	−0.68	−0.394
FYB507	0.61	30.5/19.5	189.5	55.0	−0.10	−0.132
95H	0.83	41.5/8.5	162.9	73.7	−0.25	−0.232
95G	0.78	49.0/11.0	145.6	78.7	−0.22	−0.220
95X	0.70	45.0/15.0	172.6	56.1	−0.15	−0.171

Note : $L=203$mm, $L/W=4$, $B/W=0.5$;
$W=50$mm, $B=25$mm. Side groove 20%.

$$J_{IC}=194\ (\text{KJ/m}^2) \tag{18}$$

From Fig. 5(b), the relationship of T_R versus A_2 can be fitted by a straight line

$$T_R=-187.33\,A_2+36.425 \tag{19}$$

or fitted by a 2-order curve

$$T_R=-164.77A_2^2-277.38\,A_2+25.717 \tag{20}$$

Since the small difference between the two fit curves (19) and (20) can be observed in Fig. 5(b), without the loss of generation, we only use the linear fit curve (19) in following analyses.

Based on the definition of material tearing resistance $T_R\dfrac{E}{\sigma_0^2}\dfrac{\partial J}{\partial a}\Big|_{\Delta a=1mm}$ and (19), substitution of material properties yields the slop, $\partial J/\partial a$a, of J-R curve at crack extension $\Delta a=1mm$ as

$$\frac{\partial J}{\partial a}\Big|_{\Delta a=1mm}=-350.314A_2+68.109(N/mm^2) \tag{21}$$

Since the material flow stress σ_F is the average of the material strengths, for the HY80 steel we have $\sigma_F=668$MPa. From the test results

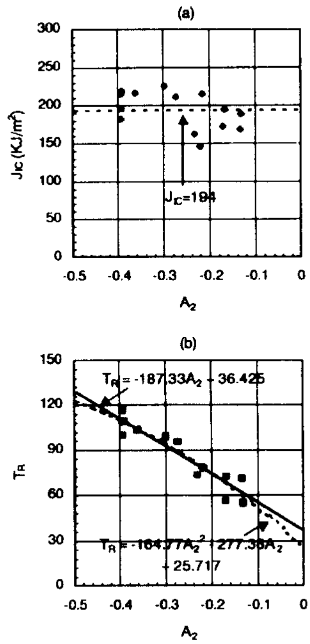

Fig. 5 Experimental data and fitting curves for SENB specimens. Note that the dots are the test data of Joyce and Link (1997), the lines are best-fit curves.
(a) Initiation toughness J_{IC} versus A_2
(b) Tearing toughness T_R versus A_2

shown in Figs. 4 and 5, $J_0\approx0$ at $\Delta a=0$ for all specimens. Thus $C_0(A_2)=0$ in (12). Then substitution of (18) and (21) into (15) gives the governing equations

$$\begin{cases} C_1(0.3452)^{C_2}=194 \\ C_1C_2=-350.31A_2+68.109 \end{cases} \tag{22}$$

For a specific value of A_2, solving (22) by Mathcad software using the non-linear Newton iteration method can obtain the magnitudes of C_1 and C_2.

For $-1.0\le A_2\le 0$, we solved (22) and plotted the relations of C_1 versus A_2 and C_2 versus A_2 in Fig. 6(a) and Fig. 6(b) denoted by dots. Two linear fitting curves follows from these two figures that

$$\begin{aligned} C_1(A_2)&=-226.35\,A_2+264.63 \\ C_2(A_2)&=-0.5813A_2+0.3182 \end{aligned} \tag{23}$$

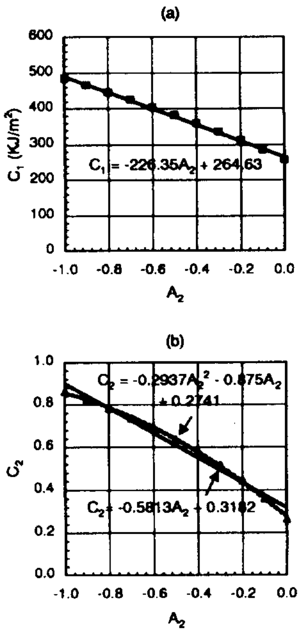

Fig. 6 Fitting curves between parameters in a constraint-corrected *J-R* curve for SENB specimens with $J_{IC}=194$ KJ/m² (the dots are the calculated data from equation (23), the line are best-fit curves).
(a) Variation of C_1 versus A_2
(b) Variation of C_2 versus A_2

Substituting (23) into (12), we obtain the constraint-corrected *J-R* curve with the parameter A_2

$$J(\Delta a, A_2)=(-226.35A_2+264.63)\left(\frac{\Delta a}{1mm}\right)^{(-0.5813A_2+0.3182)} \quad (24)$$

Figure 7 shows six different *J-R* curves predicted by (24) for $A_2=0.00$, -0.05, -0.10, -0.20, -0.30, -0.40. Comparing Fig. 7 with Fig. 3, one can find that the predicted *J-R* curves are very similar to the experimental *J-R* curves.

Figure 8 shows the comparisons between the predicted *J-R* curves by (24) and the experimental *J-R* curves tested by Joyce and Link (1997)[15] for a low constraint SENB with $a/W=0.13$ and and a high constraint SENB with $a/W=0.55$ and $A_2=-0.168$. It should be noted that in our prediction analysis of constraint-corrected *J-R* curves we only use the test data at two points within $\Delta a \leq 1$mm for a specific specimen, however, the predicted results can match very well with the experimental data up to the crack extension $\Delta a=7$mm for both shallow and deep cracks. This indicates that the J-A_2 description can indeed predict the *J*-Resistance versus crack extension within a reasonably large range of crack growth with *J* being the applied crack growing force and A_2 a constraint parameter. Therefore, this section

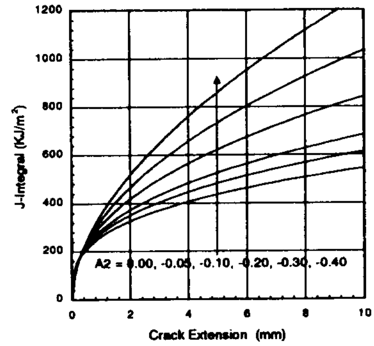

Fig. 7 *J-R* curves predicted by equation (24) for SENB specimens with $J_{IC}=194$ KJ/m² and $A_2=0.00$, -0.05, -0.10, -0.20, -0.30, -0.40.

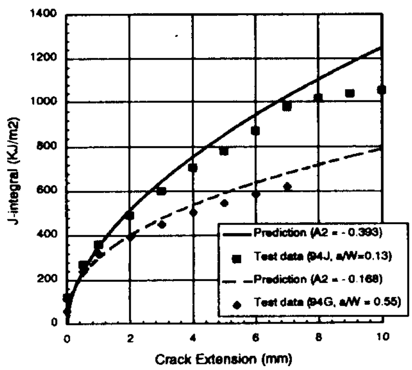

Fig. 8 Comparisons of predicted *J-R* curves by equation (24) and experimental *J-R* curves of Joyce and Link (1997) for SENB specimens with a shallow crack of $a/W=0.13$ and a deep crack of $a/W=0.55$.

shows that our approach of constraint-corrected *J-R* curves is simple and effective to predict the effect of constraint on *J-R* curves for ductile crack growth.

4. Applications of constraint -corrected *J-R* curves

For a specific material, once a constraint -corrected *J-R* curve is determined, one can apply the constraint-corrected *J-R* curves to predict the crack growth resistance for any non-standard fracture specimens or real cracked structures with the same material. This section applies the constraint-corrected *J-R* curve (24) to order the *J-R* curves for different specimen types and investigates the effect of specimen sizes on the *J-R* curves.

Consider five different conventional specimen geometries : compact tension (CT) specimen, three point bend (3PB) specimen, single edge-notched tensile (SENT) specimen, double-notched tensile (DENT) specimen and center-cracked panel (CCP), as shown in Fig. 9. The in-plane sizes of these specimens are marked in this figure, in which a is the crack depth, W is the specimen width and H or $2H$ is the specimen length. The specimen thickness is denoted by B. The five specimens are mostly common used in the fracture test.

At the level of applied J ($J=J_{IC}=194\text{KJ}/m^2$), Plane strain FEA calculations are performed for all five specimens as shown in Fig. 9 to obtain the distribution of the crack opening stress $\sigma_{\theta\theta}(r, 0)$ on the remaining ligament at the load level of $J=J_{IC}$. With the FEA results of $\sigma_{\theta\theta}(r, 0)$ and using equation (8), one can determine the magnitude of the constraint-parameter A_2 for all the specimens at the stage of initiation. In addition, the values of A_2 can be approximately determined using (16) by conversion of Q for these specimens based on the available FEA results of Q given by O' Dowd and Shih (1991, 1992)[21, 22]. For a cocnventional specimen size, e.g. the specimen width (or half of the width) $W=50$mm as recommended in ASTM fracture test standards, we obtain the constraint parameter $A_2=-0.210$, -0.241, -0.269, -0.445, -0.559 corresponding to CT, 3BP,

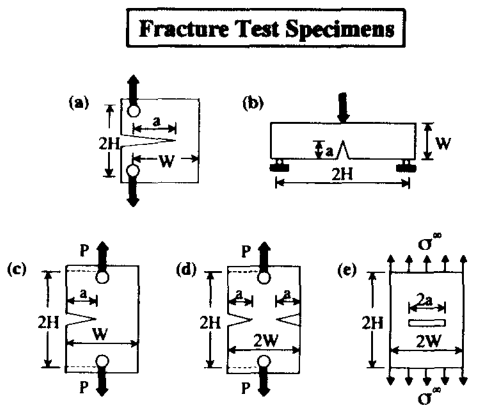

Fig. 9 Specimen geometries : (a) compact tension (CT) ; (b) three point bend (3PB) ; (c) single edge-notched tension (SENT) ; (d) double edge-notched tension (DENT) ; (e) center-cracked panel (CCP).

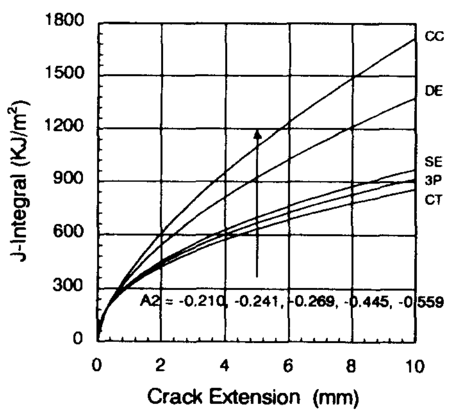

Fig. 10 Effect of specimen geometries on *J-R* curves predicted by equation (24) for conventional CT, 3PB, SENT, DENT and CCP specimens with $a/W=0.6$, $W=50$ mm and $A_2=-0.210$, -0.241, -0.269, -0.445, -0.559, respectively

SENT, DENT, CCP specimens with $a/W=0.6$. Substituting these values of A_2 into the constraint-corrected *J-R* curve (24), we can predict the *J-R* curves for all five specimens as plotted in Fig. 10. The variation trends of these predicted *J-R* curves follow those brought out in the FEA modeling work by Xia *et al.* (1995)[27] and the systematic experimental studies of the effect of constraint by Hancock *et al.* (1993)[11] and Joyce and Link (1995, 1997)[14, 15].

The deeply-cracked CT and TPB specimens have the highest constraint and lowest resistance curves, while the CCP specimen has the lowest constraint and the highest resistance curve.

To investigate the effect of specimen sizes on the *J-R* curves to ductile crack growth, we choose CT specimen as a sample and carried out FEA calculation for different specimen sizes at $J=J_{IC}$ to determine the magnitude of the constraint parameter A_2. The CT specimens we chosen cover small-sized, standard and large-sized specimens : 1/2T CT, 1T CT, 2T CT, 4T CT and 16T CT. These CT specimens have the crack depth $a/W=0.6$ and the corresponding specimen width is $W=25$ mm, 50 mm, 100 mm, 200 mm and 800 mm, respectively. Using (8), we obtain the corresponding constraint parameter $A_2=-0.406$, -0.210, -0.144, -0.118, -0.117. The *J-R* curves predicted by equation (24) are depicted in Fig. 11 for these CT specimens with the five different sizes. Note that two curves almost coincide with each other for 4T CT specimen and 16T CT specimen. This indicates that the small scale yielding deformation will maintain at the crack tip for large-sized specimen $W \geq 200$mm. Figure 11 shows that the constraint level increases and the crack tearing resistance decreases with increasing specimen size. *J-R* curves for all large-sized CT specimens are lower or flatter than that for the ASTM standard CT specimen, whereas *J-R* curve for the small-sized CT specimen is higher than that for the ASTM standard CT specimen. Hence the smaller the size of test specimens, the more dangerous or unsafe the test data for application in real cracked structures. Similar dependence of *J-R* curves on specimen sizes can be predicted using our constraint -corrected *J-R* curve (24) for 3PB, SENT, DENT and CCP specimens. These predictions are well in agreement with the FEA prediction by Xia *et al.* (1995)[27] and Shan *et al.* (1996)[25]. Therefore, one can conclude that it is unsafe for the application of *J*-*R*esistance curve data obtained from standard or small-sized specimens to large-sized specimens or real cracked structures. As a result, it is necessary and applicable to use our approach of constraint-corrected *J-R* curves to transfer and apply the laboratory *J-R* curve data into real cracked structures.

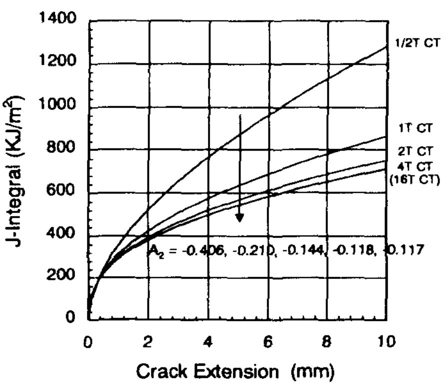

Fig. 11 Effect of specimen sizes on *J-R* curves predicted by equation (24) for 1/2T CT, 1T CT, 2T CT, 4T CT and 16T CT specimens with $a/W=0.6$ and $A_2=-0.406$, -0.210, -0.144, -0.118, -0.117, respectively.

5. Conclusions

The present paper considers the constraint effect on *J-R* curves under the two-parameter

J-A_2 controlled crack growth within a certain amount of crack extension. Both J and A_2 are used to characterize the resistance curves of ductile crack growth using J as the loading level and A_2 as a constraint parameter. The present work is summarized as follows

(1) The parameter A_2 in the J-A_2 three-term solution is independent of applied loading under fully plasticity or large-scale deformation, therefore, A_2 is a mostly proper constraint parameter at a crack tip to quantify the effect of constraints on the resistance of ductile crack growth within J-A_2 controlled crack growth.

(2) Using A_2 as a constraint parameter, the approach of constraint-corrected J-R curve is developed, and a procedure of transferring the J-R curves determined from standard ASTM measurement to non -standard specimens or real cracked structures is outlined. Provided that the constraint parameter A_2 is determined for a specific specimen, the J-R curves of this specimen can be predicted by the constraint-corrected J-R curve. Moreover, this approach can also predict the J-R curves of a surface crack in a specimen or real cracked structure. One can evaluate the variation of the constraint parameter A_2 along the front of surface crack and determine the maximum and minimum values of A_2. And then the upper and lower bound of the J-R curve for the surface crack growth can be predicted from the constraint-corrected J-R curve. This could avoid the difficult test of surface crack growth.

(3) Based on the experimental J-R curves of Joyce and Link (1997) for single-edge notched bending [SENB] specimen with from shallow cracks to deep cracks, the variation of initiation toughness JIC and tearing modulus TR with the constraint parameter A_2 is obtained. Following the procedure of constraint-corrected J-R curve presented in this work, a power-law relationship of constraint-corrected J-R curve is constructed for the test material of HY80 steel. Comparisons show that the predicted J-R curves, which only used the test data of two points within $\Delta a \leq 1mm$, can very well match with the experimental data up to the larger crack extension $\Delta a = 7mm$ for both deep and shallow cracked specimens. This shows our approach of constraint-corrected J-R curves is simple and effective to predict the effect of constraint on J-R curves for ductile crack growth. The results also indicate that the initiation toughness J_{IC} is almost a constant independent on the constraint level (A_2).

(4) This paper applies the constraint -corrected J-R curve (24) for the HY80 steel to predict the J-R curves of different conventional specimens. The order of J-R curves from high constraint to low constraint is CT, 3PB, SENT, DENT and CCP specimens, which agrees with the test results by Hancock *et al.* (1993) and Joyce and Link (1995). Specimen sizes have very serious influence on J-R curves, the constraint level increases and the crack tearing resistance decreases with increasing specimen size. Therefore, it is necessary to consider constraint effect on J-R curves when apply the laboratory J-R curve data into real cracked structures. Our approach of constraint-corrected J-R curves can do this kind of work well.

Acknowledgements

The first author would like to acknowledge the support to this work from the Mokpo National Marine University. It is also grateful to Professor Y. J. Chao in University of South Carolina for useful discussions and suggestions.

References

1) Alexander, D. J., Fracture toughness measurements with subsize Disk Compact specimens, *Small Specimens Test Techniques Applied to Nuclear Reactor Vessel Thermal Annealing and Plant Life Extension, ASTM STP 1204*, American Society of Testing and Materials, Philadelphia, 1993, pp.130~142.
2) ASTM E1737-96, *Standard Test Method for J-Integral Characterization of Fracture Toughness*, American Society for Testing and Materials, Philadelphia, 1996.
3) Betegon, C. and Hancock, J. W., Two parameter characterization of elastic-plastic crack-tip fields. *Journal of Applied Mechanics*, Vol.58, 1991, pp.104~110.
4) Brocks, W., Ebertle, A., Fricke, S. and Veith, H., Large stable crack growth in fracture mechanics specimens, *Nuclear Engineering and Design*, Vol.151, 1994, pp.387~400.
5) Chao, Y. J., Yang, S. and Sutton, M. A., On the fracture of solids characterized by one or two parameters : theory and practice, *Journal of the Mechanics and Physics of Solids*, Vol.42, 1994, pp.629~647.
6) Chao, Y.J. and Zhang, L., *Tables of plane strain crack-tip fields : HRR and higher order terms*, Me-Report, 97-1, Department of Mechanical Engineering, University of South Carolina, 1997.
7) Chao, Y. J. and Zhu, X. K., J-A_2 Characterization of Crack-Tip Fields : Extent of J-A_2 Dominance and Size Requirements, *International Journal of Fracture*, Vol.89, 1998, pp.285~307.
8) Eisele, U., Roos, E., Seidenfuss, M. and Silcher, Determination of J-integral-based crack resistance curve and initiation values for the assessment of cracked large-scale specimens, *Fracture Mechanics : twenty-second symposium (Volume I), ASTM STP 1133*, American Society for Testing and Materials, Philadelphia, 1992, pp.37~59.
9) Elliot, C., Emark, M., Lucas, G. E., et al., Development of disk compact tension specimens and test techniques for HFIR irradiation, *Journal of Nuclear Materials*, Vo01.179, Part A, 1991, pp.434~437.
10) Faleskog, J., Effects of local constraint along three-dimensional crack fronts A numerical and experimental investigation, *Journal of the Mechanics in Physics and Solids*, Vol.43, 1995, pp.447~493.
11) Hancock, J. W., Reuter, W. G. and Parks, D. M., Constraint and toughness parameterized by *T*, *Constraint effects in fracture, ASTM STP 1171*, American society of Testing and Materials, Philadelphia, 1993, pp.21~40.
12) Haynes, M. J. and Gangloff, R. P., High resolution R-curve characterization of the fracture toughness of thin sheet aluminum alloys, *Journal of Testing and Evaluation*, Vol. 25, 1997, pp.82~98.
13) Henry, B. S., Luxmoore, A. R. and Sumpter, J. D. G., Elastic-plastic fracture mechanics assessment of low constraint aluminium test specimens, *International Journal of Fracture*, Vol.81, 1996, pp.217~234.
14) Joyce, J. A. and Link, R. E., Effects of constraint on upper shelf fracture toughness, *Fracture Mechanics : 26th Volume, ASTM STP 1256*, American Society for Testing and Materials, Philadelphia, 1995, pp.142~177.
15) Joyce, J. A. and Link, R. E., Application of two-parameter elastic-plastic fracture mechanics to analysis of structures, *Engineering Fracture Mechanics*, Vol.57, 1997, pp.431-446.
16) Kikuchi, M., Study of the effect of the crack length on the J_{IC} value, *Nuclear Engineering and Design*, Vol.174, 1997, pp.41~49.
17) Klemm, W., Memhard, D. and Schmitt, W., Experimental and numerical investigation of surface cracks in plates and pipes, *Fracture Mechanics Verification by Large-Scale Testing*, EGF/ESIS8 (Edited by K. Kussmaul), 1991, pp.139~150.
18) Kordisch, H., Sommer, E. and Schmitt, W., The influence of triaxiality on stable crack growth, *Nuclear Engineering and Design*, Vol.112, 1989, pp.27~35.
19) Nikishkov, G. P., Bruckner-Foit, A. and Munz, D., Calculation of the second fracture parameter

for finite cracked bodies using a three-term elastic-plastic asymptotic expansion, *Engineering Fracture Mechanics*, Vol.52, 1995, pp.685~701.

20) Marschall, C. W., Papaspyropoulos, V. and Landow, M. P., Evaluation of attempts to predict large-crack-growth J-R curves from small specimen tests, *Nonlinear Fracture Mechanics : Volume II Elastic Plastic Fracture, ASTM STP 995*, American Society of Testing and Materials, Philadelphia, 1989, pp.123~143.

21) O' Dowd, N. P. and Shih, C. F., Family of crack-tip fields characterized by a triaxiality parameter I. Structure of fields, *Journal of the Mechanics and Physics of Solids*. Vol.39, 1991, pp.989~1015.

22) O' Dowd, N. P. and Shih, C. F., Family of crack-tip fields characterized by a triaxiality parameter II. Fracture applications, *Journal of the Mechanics and Physics of Solids*. Vol.40, 1992, pp.939~963.

23) Roos, E., Eisele, U. and Silcher, H., Effect of stress state on the ductile fracture behavior of large scale specimens, *Constraint effects in fracture, ASTM STP 1171*, American Society for Testing and Materials, Philadelphia, 1993, pp.41~63.

24) Roos, E., Eisels, U., Silcher, H. and Eckert, W., Impact of the stress state on the fracture mechanics of heavy section steel component failure mechanics, *Fracture Mechanics Verification by Large-Scale Testing, EGF/ESIS8* (Edited by K. Kussmaul), 1991, pp.65~85.

25) Shan, G. X., Kolednik, O. and Fischer, F. D., A numerical study on the crack growth behavior of a low and a high strength steel, *International Journal of Fracture*, Vol.78, 1996, pp.335~346.

26) Sharma, S.M., Aravas, N. and Zelman, Two-parameter characterization of crack tip fields in egded-cracked geometries : Plasticity and creep solutions, *Fracture Mechanics : 25th Volume, ASTM STP 1220*, American Society for Testing and Materials, Philadelphia, 1995, pp.309~327

27) Xia, L., Shih, C. F. and Hutchinson, J. W., A computational approach to ductile crack frowth under large scale yielding conditions, *Journal of the Mechanics in Physics and Solids*, Vol.43, 1995, pp.389~413.

28) Yan, C. and Mai, Y. W., Effect of constraint on ductile crack growth and ductile brittle fracture transition of a carbon steel, *International Journal of Pressure Vessels and Piping*, Vol.73, 1997, pp.167~173.

29) Yang, S., *Higher order asymptotic crack tip fields in a power-law hardening material*, Ph.D. Dissertation, University of South Carolina, 1993.

30) Yang, S., Chao, Y. J. and Sutton, M. A., Higher order asymptotic crack tip fields in a power-law hardening material, *Engineering Fracture Mechanics*, Vol.45, 1993, pp.1~20.

31) Yoon, K. K., Gross, L. B., Wade, C. S. and VanDerSluys, W. A., Evaluation of disk-shaped compact specimen for determining *J-R* curves, *Fracture Mechanics : 26th Volume, ASTM STP 1256*, American Society of Testing and Materials, Philadelphia, 1995, pp.272~283.

32) Yuan, H. and Brocks, W., Numerical investigation on the significant of J for large stable crack growth, *Engineering Fracture Mechanics*, Vol.32, 1989, pp.459~468.

33) Zhu, X. K. and Chao, Y. J., Characterization of constraint of fully plastic crack-tip fields in non-hardening materials by the three-term solution, to appear in *International Journal of Solids and Structures*, 1999.

저 자 소 개

장석기(張石基)

1951년 11월생. 1973년 한국해양대학교 기관공학과 졸업, 1988년 전남대학교 대학원 기계공학과 졸업(박사). 목포해양대학교 기관공학부 교수. 당학회 정회원.